Mon. Not. R. Astron. Soc. **000**, 1–14 (2004) Printed 2 February 2008 (MN LATEX style file v1.4)

Three-dimensional simulations of the interstellar medium in dwarf galaxies - II. Galactic winds

A. Marcolini[1], F. Brighenti[1] and A. D'Ercole[2]
[1] *Dipartimento di Astronomia, Università di Bologna, via Ranzani 1, 44127 Bologna, Italy*
[2] *Osservatorio Astronomico di Bologna, via Ranzani 1, 44127 Bologna, Italy*

Accepted ..., Received ...; in original ...

ABSTRACT

We study the hydrodynamical evolution of galactic winds in disky dwarf galaxies moving through an intergalactic medium. In agreement with previous investigations, we find that when the ram pressure stripping does not disrupt the ISM, it usually has a negligible effect on the galactic wind dynamics. Only when the IGM ram pressure is comparable to the central ISM thermal pressure the stripping and the superwind influence each other increasing the gas removal rate. In this case several parameters regulate the ISM ejection process, as the original distribution of the ISM and the geometry of the IGM-galaxy interaction. When the ISM is not removed by the ram pressure or the wind, it loses memory of the starburst episode and recovers almost its pre-burst distribution in a timescale of 50-200 Myr. After this time another star formation episode becomes, in principle, possible. Evidently, galactic winds are consistent with a recurrent bursts star formation history.

Contrary to the ISM content, the amount of the metal-rich ejecta retained by the galaxy is more sensitive to the ram pressure action. Part of the ejecta is first trapped in a low density, extraplanar gas produced by the IGM-ISM interaction, and then pushed back onto the galactic disc. The amount of trapped metals in a moving galaxy may be up to three times larger than in a galaxy at rest. This prediction may be tested comparing metallicity of dwarf galaxies in nearby poor clusters or groups, such as Virgo or Fornax, with the field counterpart. The sensitivity of the metal entrapment efficiency on the geometry of the interaction may explain part of the observed scatter in the metallicity-luminosity relation for dwarf galaxies.

Key words: galaxies: clusters: general – galaxies: dwarfs – galaxies: kinematics and dynamics – galaxies: starburst – hydrodynamics: numerical.

1 INTRODUCTION

Dwarf galaxies are key players in theories of galaxy formation. In the standard cold dark matter picture they are the first forming objects, and larger galaxies are successively built by merging of these small systems (Blumenthal et al. 1984). Given their very low metallicity and small size, these poorly evolved objects are excellent laboratories to investigate the feedback of starbursts on the interstellar medium (ISM) and to study their chemical evolution. In models of dwarf galaxies formation the feedback from supernovae (SNe) and the consequent gas and metals loss is a crucial process (Dekel & Silk 1986, Dekel & Woo 2003). The impact of starbursts in local dwarf galaxies is well studied observationally (Martin 1998, 1999; see Heckman 2003 for a recent review), but important theoretical questions remain unanswered.

A critical open problem is given by the dwarf galaxies chemical evolution. Chemical evolution models of blue compact galaxies (BCGs) (Matteucci & Tosi, 1985; Pilyugin 1992; Marconi, Matteucci, & Tosi 1994; Bradamante, Matteucci, & D'Ercole 1998; Larsen, Sommer-Larsen & Pagel 2001) indicate that the gas fraction-metallicity relations of BCGs is not compatible with the closed box scenario, suggesting that (differential) galactic winds carry away a large fraction of the metals produced by the young stars. Numerical simulations (e.g. MacLow & Ferrara 1999, D'Ercole & Brighenti 1999, Strickland & Stevens 2000, Recchi et al. 2001, 2002) and analytic models (De Young & Heckman 1994) indeed show that metals are easily ejected in the intergalactic medium (IGM). However, the details of the interaction between the metal rich hot gas and the cold interstellar medium or the IGM are yet not well understood. For instance, the mixing timescale for the metals produced in the starburst with the ISM is poorly known. Chemical evolution models often assume instantaneous mixing but HII regions

nearby star formation sites do not appear to be enriched by the young stars which illuminate them (Kobulnicky & Skillman 1996, 1997, 1998). This suggests that most of the freshly synthesized heavy elements do not mix right away with the surrounding ISM and instead reside for timescales $> 10^7$ yr in the hot ($\geq 10^6$ K) phase, where they are indeed observed (Martin, Kobulnicky & Heckman 2002). The question is then whether the hot gas leaves the galaxy and enriches the IGM or whether it eventually cools and mixes with the ISM on long timescales. The low but non-negligible metallicity of dwarf galaxies suggests that some form of mixing is effective. Possible mixing mechanisms are molecular diffusion (Roy & Kunth 1995, Tenorio-Tagle 1996, Oey 2003), condensation through thermal conduction (McKee & Begelman 1990) or turbulent mixing, likely the most important one (Bateman & Larson 1993, Roy & Kunth 1995). The close correlation between X-ray and $H\alpha$ emission also indicates some degree of thermal mixing between hot and warm gas (e.g. Lehnert, Heckman & Weaver 1999, Strickland et al. 2002).

Babul & Rees (1992) and Tenorio-Tagle (1996) proposed a scenario in which the metal enriched superbubble powered by the wind is confined by a relatively high-pressure medium and then pushed back into the galaxy. Babul & Rees (1992) suggest that the confinment is exerted by the IGM (ICM) of the group (cluster) to which the galaxy belongs. This scenario was successively investigated in more detail by Murakami & Babul (1999), who estimate that the timescale for the superbubble to collapse is of the order of a few 10^7 yr. In the model proposed by Tenorio-Tagle (1996, see also Silich & Tenorio-Tagle 2001), instead, the superbubble is halted by a hypothesized gaseous halo surrounding the galaxy. The hot gas in the bubble then cools and falls back onto the galaxy in a time-scale ~ 1 Gyr, much longer than in the models by Murakami & Babul (1999). While in their simple form these scenarios are probably too effective in retaining heavy elements (the low metal content of dwarf galaxies implies significant metal loss), some "weaker" version, where only a small but non-negligible fraction of the metal rich gas is able to cool, might help explaining the observed metallicity of dwarf galaxies.

A further complication is given by of ram pressure effect if, as expected, the galaxy moves through the IGM. It is difficult to predict the final effect of the interaction of a galactic wind with the IGM. The ram pressure could be synergic to the SN heating in removing the ISM from the galaxy. Gas lifted above the galactic plane by the SN energy may be dragged away by the IGM flow. Ram pressure effects were considered by Murakami & Babul (1999) in a number of 2D numerical simulations. These authors find that when the ram pressure of the IGM is larger than its thermal pressure, the expanding shell driven by the galactic wind is deformed, fragmenting into dense clouds eventually dragged away from the galaxy. Analogously, in the model by Tenorio-Tagle (1996) the ram pressure may strip away the hypothesized extended, loosely bound ISM, removing the medium confining the superbubble and the metals contained in it. On the other hand, may also happen that, depending on the inclination angle between the galactic plane and the orbital plane, at least one lobe of the expanding superbubble can be squashed back on the galaxy by the ram pressure. In this case the enrichment process would be more efficient compared to the case where ram pressure stripping is negligible.

Motivated by the above arguments, we have studied the interaction of starbursting dwarfs with the surrounding IGM, and how such interaction influences the evolution of the superwind powered by the stellar burst. In a previous paper (Marcolini, Brighenti & D'Ercole 2003, hereafter Paper I) we investigated the effect of the ram pressure alone on the ISM of disky dwarf galaxies. Contrary to most of the other papers devoted to this argument, we considered a ram pressure typical of galaxy groups rather than of rich clusters, because most dwarf galaxies are found in the environment of loose groups (Tully 1987). In the present paper we follow for a long timescale (500 Myr) the evolution of a galactic wind originating at the galactic centre. We focus in particular on the ejection of the ISM and of the metals synthesised in the starburst, and how their circulation is influenced by the environment and by the ram pressure.

2 THE MODEL

2.1 Galaxy models and IGM parameters

We consider three galaxy models, described in detail in Paper I, differing for their masses and indicated with SM (small), MD (medium) and LG (large). The gravitational potential is due to a spherical quasi-isothermal dark matter halo and a stellar thin Kuzmin's disk. As in Paper I we defined two regions: the *galactic region* and the *central region*. The first is representative of the whole galaxy and is defined as a cylindrical volume within $z < |z_{\rm gal}|$ and $R < R_{\rm gal}$ (where z and R are the usual cylindrical coordinates). The second, smaller region samples the central region where most of the stars are located ($z < |z_{\rm centr}|$ and $R < R_{\rm centr}$); the masses of the gas content in these two regions are indicated as $M_{\rm gal}$ and $M_{\rm centr}$, respectively. The masses of the dark halo, stellar disk and initial ISM (before stripping) are summarized in Table 1.

The ram pressure effects are studied assuming two sets of density-velocity combination for the IGM: the first with $(\rho_{\rm IGM}, v_{\rm IGM}) = (2 \times 10^{-28} {\rm g\,cm^{-3}}, 200\ {\rm km\,s^{-1}})$ called LO (low), and the second with $(\rho_{\rm IGM}, v_{\rm IGM}) = (2 \times 10^{-27} {\rm g\,cm^{-3}}, 400\ {\rm km\,s^{-1}})$ called HI (high). The IGM temperature is $T_{\rm IGM} = 10^6$ K.

In Paper I we run 18 simulations of rotating dwarf galaxies undergoing ram pressure stripping, varying the galactic mass, the ram pressure strength, and the inclination angle θ between the galactic plane and galactic velocity. We identified a particular model with the notation XX-YY-ZZ, where XX individuates the galaxy size (SM, MD, LG); YY expresses the angle θ, and takes the values YY=00 for edge-on models, YY=45 for $\theta = 45^\circ$, and YY=90 for face-on models. Finally, ZZ represents the value of the ram pressure; ZZ=LO for the weak ram pressure, ZZ=HI for the high one. In the present paper we do not consider the models SM-HI (for every inclination angle), MD-45-HI and MD-90-HI because they quickly lose their ISM during the stripping phase, and no galactic wind can occur (cf. Paper I).

The initial conditions for the gas in the present simulations are given by of the final outputs of Paper I, where the gas distribution has been modified by the effect of the ram pressure stripping lasting for 1 Gyr.

Table 1. Initial galaxy model parameters

Model	M_* ($10^8\,M_\odot$)	$M_{\rm h,tot}$ ($10^9\,M_\odot$)	$M_{\rm centr}$ $^{(a)}$ ($10^7\,M_\odot$)	$M_{\rm gal}$ $^{(b)}$ ($10^8\,M_\odot$)	$R_{\rm centr}$ (kpc)	$\lvert z_{\rm centr}\rvert$ (kpc)	$R_{\rm gal}$ (kpc)	$\lvert z_{\rm gal}\rvert$ (kpc)
SM	0.6	0.76	0.9	0.5	1.0	0.5	4.0	1.0
MD	6.0	7.4	6.6	4.1	2.0	1.0	8.0	2.0
LG	60.0	77.2	42.2	33.1	4.0	2.0	16.0	4.0

$^{(a)}$ initial ISM mass content of the central region defined as a cylinder with $R < R_{\rm centr}$ and $z < |z_{\rm centr}|$.
$^{(b)}$ initial ISM mass content in the galactic region defined as a cylinder with $R < R_{\rm gal}$ and $z < |z_{\rm gal}|$.

2.2 The starburst

We assume an instantaneous burst of star formation which injects energy into the ISM for a period of 30 Myr, approximately the lifetime of an $8M_\odot$ star, the smallest star producing a Type II SN. We assume that the starburst produces a steady mechanical energy input rate of $L_{\rm inp} = 3.8 \times 10^{40}{\rm erg\,s^{-1}}$, which is a mechanical power similar to the lower limit estimated for NGC 1569 (Heckman et al. 1995). The mass injection rate is assumed to be $\dot{M} = 3 \times 10^{-2} M_\odot\,{\rm yr}^{-1}$. The total energy deposited after 30 Myr is then $\sim 3.6 \times 10^{55}$ erg and the total mass returned to the ISM by stellar winds and SNII is $M_{\rm ej,tot} = 9 \times 10^5 M_\odot$ (cf. D'Ercole & Brighenti 1999). According to Leitherer & Heckman (1995) the assumed injected energy corresponds to an instantaneous starburst of $\sim 2 \times 10^6$ M$_\odot$.

2.3 The numerical simulations

We solve the usual hydrodynamic equations, with the addition of a mass source term and a thermal energy source term; the injected hot gas expands to form the starburst wind with the appropriate mechanical luminosity $L_{\rm inp}$. The constant mass and energy source terms for unit volume are given respectively by $\dot{\rho} = \dot{M}/\mathcal{V}$ and $\dot{\epsilon} = L_{\rm inp}/\mathcal{V}$, where $\mathcal{V}$ is the volume of the source region, chosen to be a sphere with a radius of 80 pc and located in the galactic centre. In order to follow the circulation of the metals produced in the starburst we solve an additional continuity equation for the stellar ejecta density $\rho_{\rm ej}$ (which is then advected passively).

The simulations shown in Paper I did not take into account radiative losses. In fact, it can be shown that such losses are generally not important during the gas stripping. During the wind phase, instead, the ISM compressed by the wind has rather short cooling times and radiative losses must be included in the models. We use a fit for the cooling function given in Sutherland & Dopita (1993), for solar abundances.

In order to achieve a better spatial resolution we remapped the final outputs of Paper I on a finer grid, with twice the number of zones in every direction. In the present paper the simulations are calculated on a grid with 212^3 meshes ($212 \times 212 \times 108$ meshes for edge-on models with planar symmetry). The grid size has a geometrical progression in all directions with central zones $\Delta x = \Delta y = \Delta z = 20$ pc, with size ratio between adjacent zones of 1.0425.

Table 2. Characteristic ISM values at the beginning of the starburst

Model	θ (°)	$M_{\rm centr}$ ($10^7\,M_\odot$)	$M_{\rm gal}$ ($10^8\,M_\odot$)	$\overline{R}_{\rm ISM}$ (kpc)
	0	0.88	0.30	2
SM-LO	45	0.91	0.25	2
	90	0.74	0.19	2
	0	0.	0.	0
SM-HI	45	0.	0.	0
	90	0.	0.	0
	0	6.80	3.77	8
MD-LO	45	6.31	3.24	6
	90	6.17	3.28	6
	0	3.84	0.66	2
MD-HI	45	0.	0.	0
	90	0.	0.	0
MD-HIbis	0	9.97	3.44	3
	0	43.0	33.0	22
LG-LO	45	42.8	32.9	19
	90	42.2	32.6	18
LG-HIbis	0	62.5	26.5	6
LG-HI	45	25.7	3.3	2
	90	10.2	1.0	2

3 RESULTS

Anticipating the results presented below, we stress the importance of the ISM flare at large radii in our galaxy models. The flare of the initial gas distribution is due to our assumption of isothermal equilibrium of the unperturbed rotating ISM. Such a flare does not affect the evolution of the galactic winds occurring in the centre of a galaxy at rest. However, the ISM stripped from the leading edge of a galaxy moving through an external medium may form a sort of extraplanar gaseous halo surrounding the inner galactic region. Thus, the galactic wind propagation is not only affected by the direct impact of the ram pressure (at larger z), but also by the possible presence of such an halo (at smaller z). The halo is more substantial for larger galaxies and for larger values of ram pressure and, for geometrical reasons, this effect is more significant for edge-on models.

Below we describe in some detail the gasdynamics of the models, paying a special attention to the galaxy MD, our reference model.

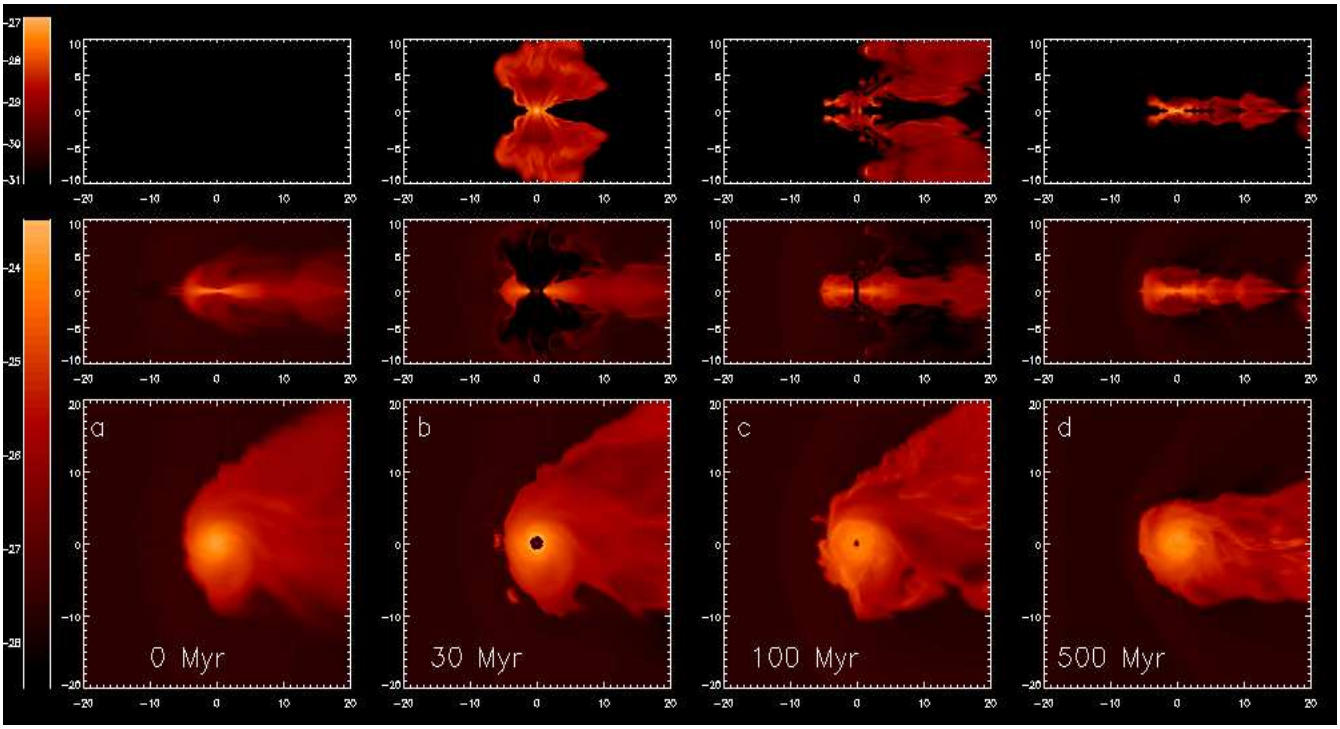

Figure 1. Density distribution of the ISM and the ejecta in the reference model MD-00-LO at several times. The intermediate and lower rows illustrate the ISM distribution on the galactic plane ($z = 0$) and meridional plane ($y = 0$), respectively. The upper row refers to the ejecta distribution in the meridional plane. The distances are given in kpc.

3.1 The reference model

3.1.1 Model MD-00-LO: hydrodynamics

In Fig. 1 several snapshots of the gas distribution for model MD-00-LO are shown at different times; the second and the third rows refer to the ISM distribution in the meridional and galactic plane respectively, while the first row refers to the SN-ejecta distribution in the meridional plane. The IGM enters the grid from the left boundary and moves toward the right.

The first column shows the gas density distribution just before the starburst episode ($t = 0$). As the SNe start to explode, a superbubble expands supersonically through the ISM, giving rise to the classical two shocks configuration. The reverse shock interacts with the freely expanding wind which is heated to $T \geq 10^7$ K. As the outer shock propagates the ISM is compressed into a shell. This shell quickly breaks out and accelerates along the z direction as it moves through a less dense environment. The bubble as a whole acquires the classical bipolar shape. As a consequence of the acceleration, the shell becomes Rayleigh-Taylor (RT) unstable and fragments.

The second column of Fig. 1 represents the wind evolution at $t = 30$ Myr, the time at which the SNe activity ceases. At this time the central hole carved in the ISM reaches its maximum extension of $R \sim 1$ kpc; an hole of approximately this size has been effectively observed, for example, in Holmberg I (Ott et al. 2001, Vorobyov et al. 2003). Along the z direction the wind expands freely to much larger heights and the shape of the reverse shock is not spherical; similar structures are found by D'Ercole & Brighenti (1999), Mac Low & Ferrara (1999) and Strickland & Stevens (2000) for models with thin gaseous disks. The shell of shocked IGM, with density $\rho \sim 6.3 \times 10^{-28}$ g cm^{-3} and temperature $T \sim 2.2 \times 10^6$ K, never cools to form a thin dense structure as it does when the superbubble is expanding within the ISM. At $t = 30$ Myr the outer shock has reached a distance $z \sim 12$ kpc above the galactic plane and has a velocity of ~ 230 km s^{-1} along the $z-$axis. At this stage the effect of the IGM ram pressure is not yet substantial and the superbubble is still quite axially symmetric around the $z-$axis. As the energy injection stops, the pressure of the hot gas decreases by expansion (and by radiative losses occurring at the numerically broadened interfaces between hot and cold gas) and the ram pressure drags the gas expelled by the galaxy downstream.

At $t = 100$ Myr (Fig. 1, panels *c*) most of the gas at high z is moved behind the galaxy. The central hole in the ISM is still present, but it will be filled up by the cold gas on the galactic plane which recollapses toward the centre. When this happens (at $t \sim 250$ Myr) another central starburst might occur (D'Ercole & Brighenti 1999).

The last column of Fig. 1 (panels *d*) shows the gas distribution at $t = 500$ Myr. The ISM in the central region has almost recovered its initial distribution, although the gas density at the centre is somewhat lower than that at $t = 0$. This is due to the ejection of the low angular momentum-gas initially located in the very centre of the galaxy. The ISM which flows in the central region at later time has higher angular momentum and does not reach the very centre because of angular momentum conservation. Overall, the galaxy has the classic cometary shape, typical of galaxies undergoing

Table 3. Ejecta masses in the central region

Model	$M^{\rm cold}_{\rm ej,centr}$ $(10^3 M_\odot)$				$M_{\rm ej,centr}$ $(10^3 M_\odot)$			
	10 Myr	30 Myr	100 Myr	500 Myr	10 Myr	30 Myr	100 Myr	500 Myr
LR,COOL	29.9	38.3	24.1	47.3	55.1	65.1	24.1	49.4
LR,NO-COOL	6.88	5.86	0.94	1.86	35.0	35.8	0.95	1.88
HR,COOL	25.2	32.7	25.2	42.9	50.6	59.6	25.3	43.0

The total ejecta mass for $t \geq 30$ Myr is 9×10^5 $M_\odot$.

ram pressure stripping (Paper I and references therein). The tail becomes narrower with time, an indication that the system is not in a steady state.

Fig. 5 shows the evolution of $M_{\rm centr}$ and $M_{\rm gal}$ before the starburst (discussed in Paper I) and following it. The temporary decrease of the ISM mass occurring at ~ 1 Gyr (i.e. when the starburst occurs) in the central region is due to the galactic wind. As the energy injection stops, the mass gas increases again. The gas mass inside the central region at the end of the simulation is slightly larger than its initial value. This is due to gas ablated from the leading edge of the galaxy by the ram pressure which later falls in the central region.

3.1.2 Model MD-00-LO: SN ejecta evolution

In this section we investigate the fate of the metals injected by the SNe created by the starburst. This task, however, is severely hampered by the effects of the numerical diffusion, which artificially mixes the SNe ejecta and the cold ISM. This is a well known problem, discussed for example in D'Ercole & Brighenti (1999), Recchi, Matteucci & D'Ercole (2001) and de Avillez & Mac Low (2002). Generally, the real mixing processes as molecular diffusion (e.g. Oey 2003), condensation by thermal conduction (e.g. McKee & Begelman 1990) or turbulent mixing (Begelman & Fabian 1990, Bateman & Larson 1993) are less effective than the numerical diffusion which affects our simulations. Therefore, our calculations likely provide an upper limit to the amount of metals trapped in the ISM. Thus, before to describe the evolution of the SN ejecta in model MD-00-LO, it is useful to make a brief digression on the influence of the numerical diffusion on the mixing of the hot metal rich material.

To study quantitatively the numerical mixing we consider as a fiducial model a (2D) galactic wind in the reference galaxy described above, but now assumed at rest (i.e. no ram pressure) to simplify the interpretation of the results. Fig. 2 illustrates the evolution in the meridional plane of the gas density (black contours) and the ejecta density (red contours) for this model. The top row shows the model calculated at the same resolution of models MD-00-LO, at $t = 10$, 30 and 500 Myr. This model includes radiative cooling and will be indicated in the following as LR,COOL. The three snapshots clearly show how the ejecta penetrates the cold ISM. In Table 3 we list the cold ($T < 10^5$ K) and the total mass of the ejecta ($M^{\rm cold}_{\rm ej,centr}$ and $M_{\rm ejcentr}$) in the central region for the various models described in this section. In absence of numerical diffusion we would expect $M^{\rm cold}_{\rm ej,centr} = 0$, since the radiative cooling time of the ejecta is longer than the age of the wind.

We find that after the energy injection stops (at $t = 30$ Myr) essentially all the ejecta found in the central region is cold, as a result of numerical diffusion. In the third row of Fig. 2 we show the same model calculated with higher resolution (model HR,COOL). The linear grid size in the relevant region (say at ~ 1 kpc from the centre) is now about 3 times smaller than in model LR,COOL. From Table 3 we see that, somewhat unexpectedly, increasing the resolution does not reduce the amount of the diffused ejecta. We note that de Avillez & Mac Low (2002) similarly found that the mixing timescale of chemical inhomogeneities in their models for the Galactic ISM was rather insensitive on the numerical resolution.

The effect of the radiative cooling is instead crucial. In the second row it is shown the low resolution model calculated with the radiative cooling turned off (model LR,NO-COOL). Now $M^{\rm cold}_{\rm ej,centr}$ and $M_{\rm ej,centr}$ are greatly reduced with respect to models LR,COOL and HR,COOL. At late times, in models without radiative cooling the central region hosts less than 5 % of the ejecta mass present in the analogous models which include radiative losses (a high resolution model without radiative losses, not shown here, gives similar results). Evidently when radiative losses are included, the ejecta cools at the numerically broadened interfaces between hot and cold gas. We must conclude that the majority of the ejecta trapped in the ISM in our models is due to the combination of numerical diffusion and radiative cooling. Thus, we consider the results of our simulations as an upper limit of the mixing efficiency.

We now come back to model MD-00-LO. The upper panels of Fig. 1 show the evolution of the ejecta density in the plane $x-z$, while the time evolution of the ejecta masses $M_{\rm ej,centr}$ and $M_{\rm ej,gal}$, defined similarly to the gas masses in the section 2.1, is shown in Fig. 7 (solid line). Initially, the mass of the ejecta increases as it is delivered by SNe. Successively, at $t > 30$ Myr, the ejecta close to the galaxy continues to move vertically leaving the central region and causing the minimum in $M_{\rm ej,centr}$ seen in Fig. 7 at ~ 100 Myr. The ejecta which reaches large heights ($z \geq 2-3$ kpc) is effectively dragged away by the ram pressure (Fig. 1, panels *c*). However, some of the ejecta surrounding the galaxy is pushed back onto the galactic plane together with the ISM stripped from the leading edge of the galaxy, as discussed above. As a consequence, $M_{\rm ej,centr}$ increases again before to attain a nearly constant value at $t \sim 200-300$ Myr. At the final time $t = 500$ Myr about 4% of the metals produced in the starburst is within the central region.

The evolution of $M_{\rm ej,gal}$ shows less variation with respect to $M_{\rm ej,centr}$ because of the larger volume involved (see Fig. 7). After $t = 30$ Myr about a constant fraction $\sim 8\%$ of

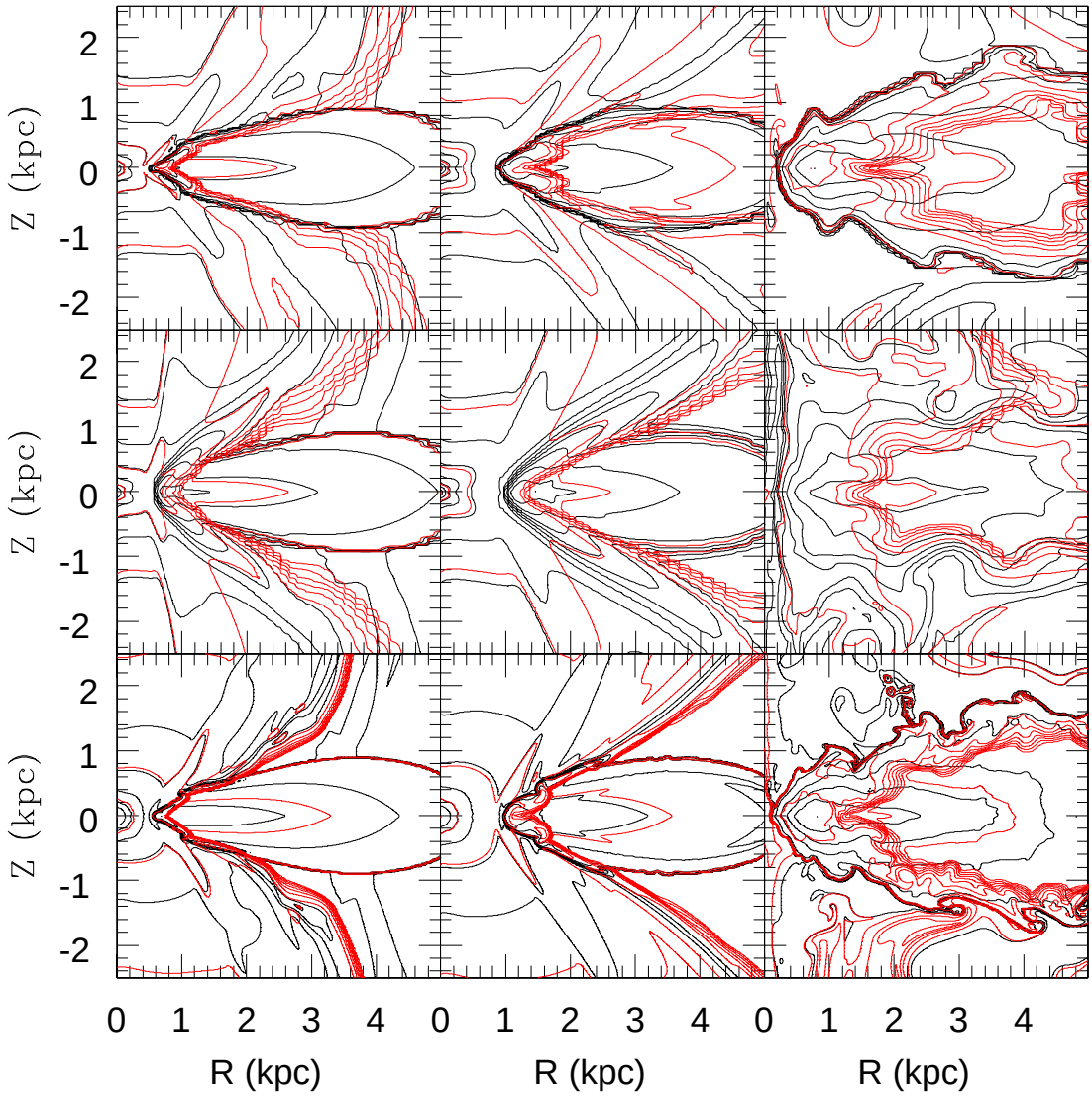

Figure 2. Gas (black contours) and ejecta (red contours) distributions for the 2D model MD at rest for different grid resolutions, with and without radiative cooling. From top to bottom the rows refer to models LR-COOL, LR-NOCOOL, HR-COOL respectively. From left to right the columns refer to $t = 10$ Myr, $t = 30$ Myr and $t = 500$ Myr, respectively. Given the symmetry of the model each panel shows only half of the meridional plane. The z-axis coincides with the symmetry axis.

the total ejecta mass is located in the galactic region. Almost all the ejecta inside both the galactic and the central regions has cooled off and condensed onto the ISM for $t \geq 100$ Myr. It is located along the edges of the ISM (Fig. 1) and it is unaffected by the ram pressure. The vast majority of the ejecta is thus lost definitively by the galaxy and pollutes the IGM.

3.1.3 Models MD-45-LO and MD-90-LO

The first column in Fig. 3 represents the gas distribution of model MD-45-LO at the beginning of the burst. The IGM enters the grid from the left and from the top and moves in the diagonal direction. Downstream (i.e. for $z < 0$) the ablated ISM forms a gaseous halo close to the galaxy. Thus, as the wind starts to blow, the upper lobe of the superbubble expands through a less dense medium ($\rho = 3 \times 10^{-28}$ g cm^{-3}) compared to the gas surrounding the lower lobe ($\rho = 1 - 2 \times 10^{-27}$ g cm^{-3}). As a consequence it expands faster despite the decelerating action of the ram pressure. During the SNe activity ($t \leq 30$ Myr) the ram pressure is comparable to the superbubble pressure at large distance ($z > 4$ kpc), where the symmetry between the two lobes breaks. The density distribution at $t = 30$ Myr is illustrated in the second column of Fig. 3. From the ejecta distribution (upper panel) one can see that the downstream lobe

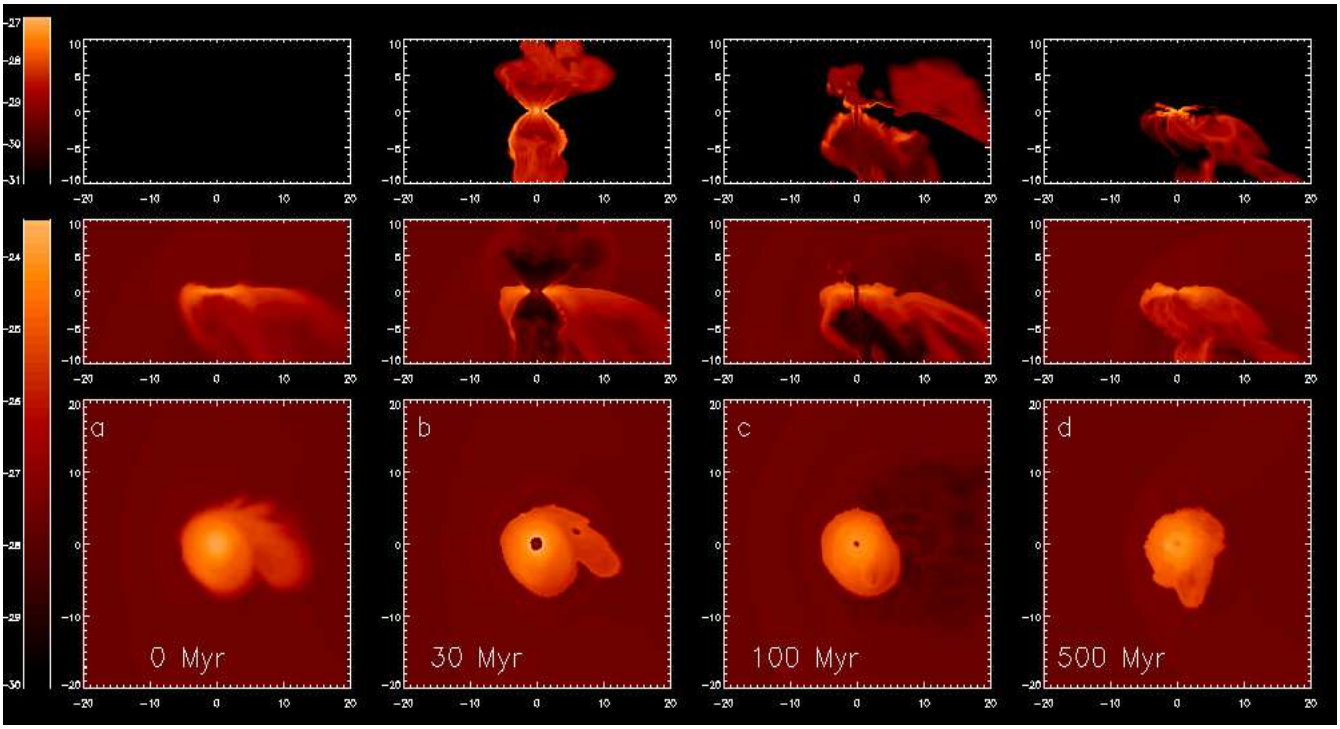

Figure 3. The same as in Fig. 1 but for the model MD-45-LO.

has reached larger heights (~ -15 kpc) compared to the upper lobe (~ 12 kpc). The last two columns of Fig. 3 show the successive evolution of the ISM and the ejecta. The latter is progressively dragged downstream and at late times no ejecta is present "above" the galaxy. As for model MD-00-LO, the ISM loses memory of the starburst episode and almost recovers its initial distribution at $t \sim 200$ Myr.

Fig. 4 shows the gas evolution of the model MD-90-LO. The IGM enters the grid from the upper grid boundary. Given the symmetry of this configuration with respect to the $z-$axis, we have run this simulation on a 2D grid in cylindrical coordinates, with the same resolution as the previous calculations. In this model the superbubble lobe expanding upstream is smaller than the opposite lobe because of the ram pressure. At $t \sim 30$ Myr the outer shock propagating upstream overtakes the bow shock created by the motion of the galaxy (located at $z \sim 10$ kpc) and reaches the maximum distance $z \sim 14$ kpc at $t \sim 40$ Myr. Upstream, the density and temperature of the shocked IGM at $t = 30$ Myr are $\rho \sim 6 \times 10^{-28}$ g cm^{-3} and $T \sim 2.5 \times 10^6$ K, respectively. In the downstream direction, the forward shock exits the boundary of the grid at $t \sim 20$ Myr. The reverse shocks are located at $z \sim 3$ kpc upstream and at $z = -8$ kpc downstream and the shocked gas has temperature $T \sim 2-4 \times 10^7$ K. On the galactic plane ($z = 0$) the outer and reverse shocks have a radius of ~ 1 and ~ 0.7 kpc, respectively. The density and temperature of the shocked wind are $\sim 2.5 \times 10^{-28}$ g cm^{-3} and 7×10^7 K, respectively.

As the SNe activity ceases, the ejecta expelled upstream is pushed back toward the galaxy. However, most of it moves around the galaxy and is lost downstream. The ISM collapses back in the central region at $t \sim 100$ Myr. However, a central small hole is always present and some of the external gas moving toward the galaxy goes through this hole which has a radius of ~ 300 pc (see also Quilis, Moore & Bower 2000).

The evolution of $M_{\rm centr}$ and $M_{\rm gal}$ is quite similar for all models MD-LO (Fig. 7), although $M_{\rm gal}$ assumes slightly larger values for the edge-on model. Also the behaviour of $M_{\rm ej,centr}$ and $M_{\rm ej,gal}$ is similar for all models MD-LO, with no clear dependence on θ. This point will be discussed further in section 5.2.

Model MD-90-LO, being calculated on a 2D grid, is computationally inexpensive and it is therefore well suited for a numerical convergence study. We have recalculated this model on a finer grid with central zone size of 10×10 pc^2, and size ratio between adjacent zones 1.00447. The total number of zones is thus 1200×600. Although, as expected, many small scale structures are present in the high resolution simulation, the overall dynamical evolution of the galactic wind is very similar to that of the low resolution model. The evolution of $M_{\rm centr}$, $M_{\rm gal}$ and the ejecta masses is also very similar at high and low resolution. At $t = 500$ Myr, $M_{\rm ej,centr}$ and $M_{\rm ej,gal}$ for the low resolution model is only $\lesssim 20\%$ larger than in the high resolution one, consistently with the experiments on the numerical diffusion described in section 3.1.2. We conclude that the relatively low numerical resolution of our models does not affect the global evolution of the ISM and the SN ejecta.

3.2 Models MD-HI

We now discuss the evolution of a galactic wind in the same galaxy model described in the previous section, but in the

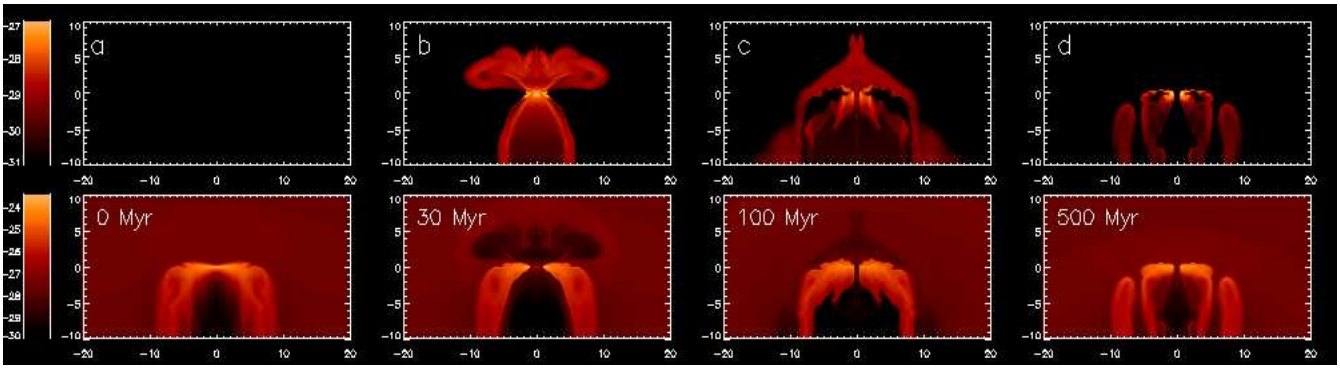

Figure 4. Density distribution of the ejecta (upper panels) and the ISM (lower panel) in model MD-90-LO in the meridional plane at several times. The distances are given in kpc.

case of a higher ram pressure (HI). As shown in Fig. 5 and discussed in Paper I, for model MD-00-HI the ram pressure phase before the starburst results in a loss of $\sim$ 80 % of the original ISM in the galactic region. In the central region the effect is milder and only $\sim$ 40 % of the gas is removed. Because of the lower ISM content, the galactic wind is now able to remove completely the remaining ISM after $t \sim 200$ Myr since the burst occurrence. Its worthwhile to note that, even in absence of a central starburst, the ISM would have been completely removed by the ram pressure at $t \sim 700$ Myr (i.e. after 1.7 Gyr from the beginning of the stripping). Therefore, the wind anticipates the total stripping of the gas by $\sim$ 500 Myr. A scenario in which both SNe energy and ram pressure stripping act together to remove the ISM is argued by Gallart et al. (2001) for the Phoenix dwarf galaxy.

The duration of the ram pressure stripping phase, 1 Gyr, is arbitrary. Such a time interval is comparable or longer than the crossing time of a typical group (a few 10^8 yr). Therefore, if the starburst episode is triggered by tidal interactions with other galaxies, or by the ram pressure itself (see Paper I), it may occur after a shorter lapse of time. In this case the superbubble can interact with a more massive ISM and its evolution can change somewhat. In order to investigate this point, we run a model MD-00-HIbis, identical to MD-00-HI, but taking as initial condition the ISM configuration at 190 Myr since the beginning of the stripping phase. At this time the ISM mass content in the central region is maximum, $M_{\rm centr} \sim 1.0 \times 10^8\ M_\odot$ (see Fig. 5), and possible differences in the bubble evolution are expected to be larger. Fig. 5 shows the evolution of $M_{\rm centr}$ and $M_{\rm gal}$ for both model MD-00-HI and model MD-00-HIbis. In model MD-00-HIbis the more massive ISM prevents the complete evacuation of the galaxy, contrary to model MD-00-HI.

In Fig. 7 the evolution of $M_{\rm ej,centr}$ and $M_{\rm ej,gal}$ for the two models MD-00-HI is compared . As it is immediately apparent from this figure, much more ejecta is trapped into the galaxy in the model MD-00-HIbis during the first 200 Myr. This is due to the fact that the superbubble is expanding in a medium which is on average $\sim$ 3 time denser and suffers larger radiative losses at the interfaces between hot and cold gas. The ejecta is successively stripped together with the ISM. After 230 Myr the metal content becomes similar to that of model MD-00-LO indicating that the galactic metal enrichment is not affected by the ram pressure in the long run.

As shown in Paper I, models MD-45-HI and MD-90-HI are completely deprived of ISM after a time $\sim 200-400$ Myr, comparable to the dynamical timescale of a galaxy group. Therefore we did not make any galactic wind simulation in these models.

4 OTHER MODELS

4.1 Models SM

Although during the ram pressure phase models SM-LO retain almost all of the ISM in the central region and approximately 40-60% of the gas in the galactic region, the ISM is easily blown away by the galactic wind for any inclination angle (see Fig. 5). Winds in the models SM-HI have not been simulated because they are quickly deprived of gas by the ram pressure (cf. Paper I).

4.2 Models LG

4.2.1 LG-LO

As for models MD-LO, also for the more massive galaxy models LG-LO the evolution of the gas content is rather insensitive to the inclination angle θ. Contrary to model MD-LO, instead, the onset of the SNe activity does not produce any significant decrease of $M_{\rm centr}$. This is due to the fact that the central region for the LG model includes a larger volume, while the central hole carved by the wind is narrower ($\sim$ 800 pc in radius) because of the denser ISM.

The amount of metals trapped in the LG-LO models is generally larger than in models MD-LO. This is explained by the more massive extraplanar halo of stripped ISM present in models LG-LO which efficiently contrasts the expansion of the superbubble. This effect is particularly dramatic for $\theta = 0$, when the trapped ejecta is maximum. The presence of the halo increases the value of the critical luminosity needed by the wind to break out (e.g. Mac Low, McCray & Norman 1989, Koo & McKee 1992; see also Section 5.3). In the LG-LO-00 model the wind luminosity is quite close to the critical value, as discuss in section 5.3. As a consequence, part of the

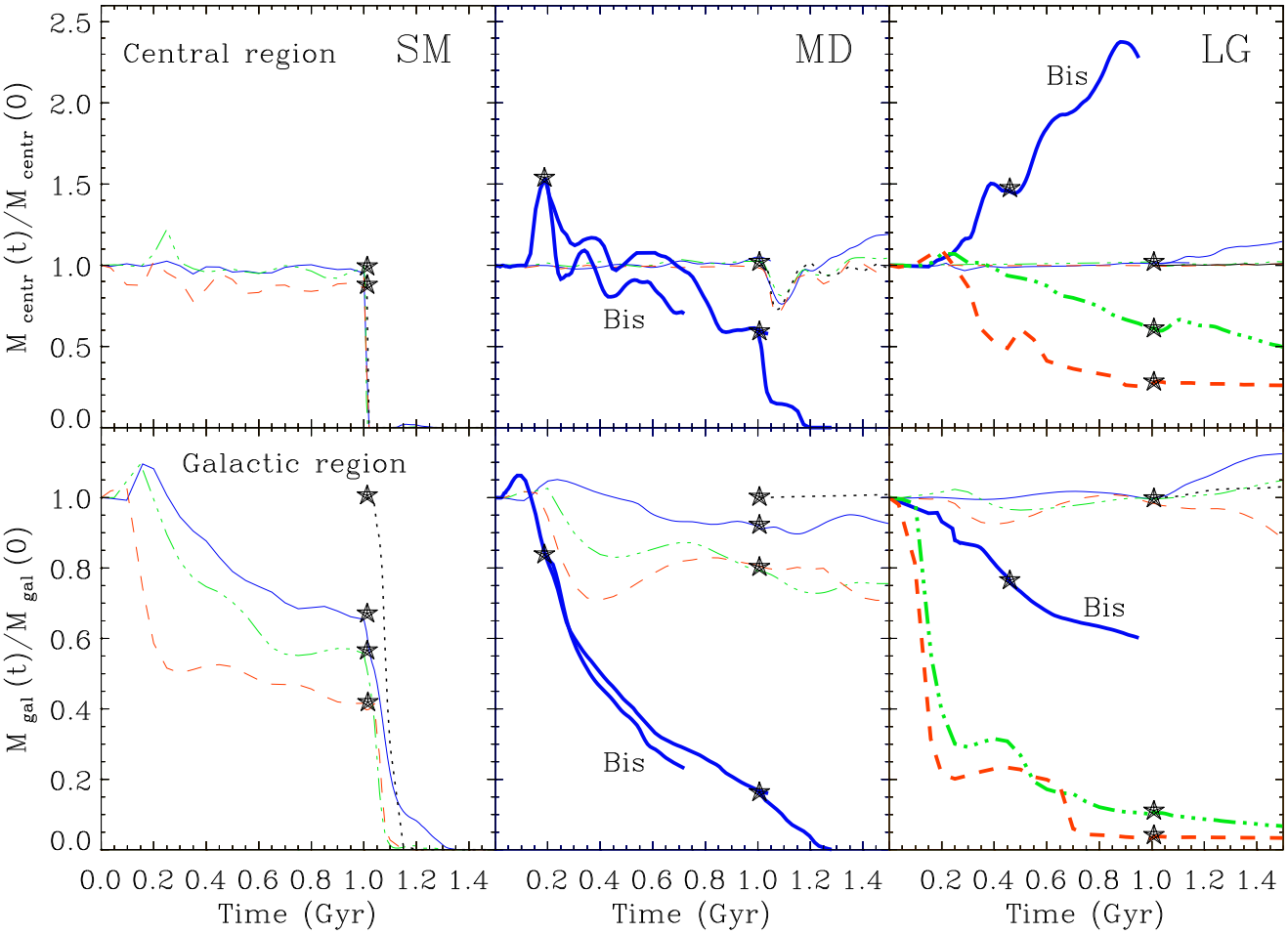

Figure 5. Evolution of the cold ($T < 3 \times 10^5$ K) ISM mass in the "central region" (upper panels) and in the "galactic region" (lower panels). From left to right the couples of lower and upper panels refer to SM, MD and LG models respectively. Solid blue lines: edge-on models; dashed-dotted green lines: 45° models; dashed red lines: face-on models; dotted lines: REST models. Light and heavy lines refer to LO and HI ram pressure models, respectively. Being the FIELD models very similar to the REST models we do not report them in the picture for the sake of clarity. The evolution of the masses is reported over a time interval of 1.5 Gyr: during the first 1 Gyr (with the exception of models Bis, see text) the masses evolve only under the action of the ram pressure (Paper I). The occurrence of the starburst is indicated by a star.

wind gas remains trapped in the halo and falls back on the galactic disk together with collapsing halo itself.

A further reason for the larger values of $M_{\rm ej,centr}$ and $M_{\rm ej,gal}$ in models LG-LO is the large size of the ISM disk, which intercepts a larger amount of the metal rich gas pushed back by the ram pressure. This effect is especially important for the LG-LO-90 model.

4.2.2 LG-HI

As pointed out in section 2.3, the stripping simulations of our models in Paper I are adiabatic because, as stated in that paper, radiative losses are usually negligible. However, in the case of the model LG-00-HI this is not completely true. In this model the ISM flare influences more strongly the stripping evolution. The extraplanar gaseous halo formed around the LG-00-HI model is dense enough to make the radiative losses not negligible. In order to make a self consistent model we run again LG-00-HI taking into account the radiative cooling *ab initio*, i.e. also during the ram pressure stage (model LG-00-HIbis). Given the smaller time step (due to the radiative time scale), we run this simulation only up to 500 Myr. In this case part of the halo is able to cool and to fall on the central region of the galactic plane, increasing $M_{\rm centr}$. The radiative halo is more clumpy and filamentary than the adiabatic halos forming in the previous models. The massive, radiative extraplanar halo also explains why model LG-00-HIbis retains much more metals than any other model. The cooled off and fallen halo material is polluted with metals carried at high z by the wind and mixed with the halo gas. This process is ultimately a consequence of the ram pressure and may result in a different chemical evolution for galaxies moving through an IGM with respect to isolated objects.

¿From Figure 5 we see that the rate of mass loss for models LG-45-HI and LG-90-HI is not significantly altered by the occurrence of the starburst. Evidently the time evolution of $M_{\rm centr}$ and $M_{\rm gal}$ is regulated by the ram pressure

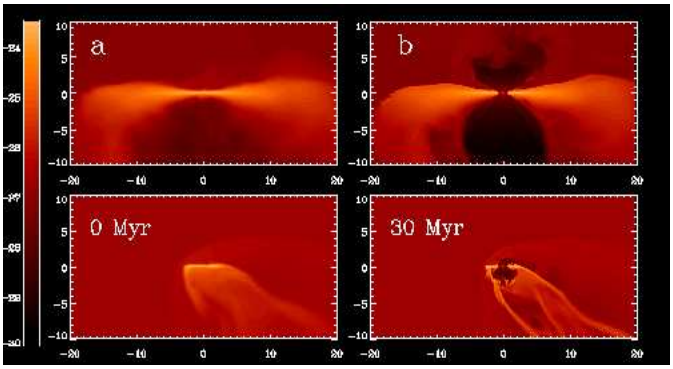

Figure 6. Density distribution of the ISM for the two large 45° models with low ram pressure (LG-45-LO; upper panels) and high ram pressure (LG-45-HI; lower panel). The first and the second column refer to the initial condition at the beginning of the starburst (0 Myr) and the end of it (30 Myr), respectively. The distances are given in kpc.

alone. This also indicates that in these models the gaseous halo, less massive than in model LG-00-HI, does not radiate efficiently. In fact, because of the different geometry, the influence of the ISM flare is much less important for the LG-45-HI model and negligible for LG-90-HI model, where no substantial gaseous halo is present. In model LG-45-HI (shown in Figure 6), the halo surrounds only the downstream side of the galaxy.

The dependence on θ of the extraplanar halo formation induces a dependence on θ of the evolution of $M_{\rm ej,centr}$ and $M_{\rm ej,gal}$ (see Fig. 8), because larger haloes lead to larger amounts of trapped ejecta. Moreover, a secondary reason for this θ-dependence is given by the fact that inclined galaxies have smaller radii (see Tab. 2) because of the ram pressure truncation, and thus are less able to retain metals pushed back on the galactic disk.

The above arguments also explain why an analogous dependence on θ is less pronounced in the case of lower ram pressure. In this latter case the size of the gaseous galactic disk is less affected by the inclination angle, and, more important, extends to a larger R. As a consequence, the gas stripped from the galactic edge is less dense and moves at higher z over the galactic centre, opposing a weaker contrast to the superwind expansion. This is clearly shown in Fig. 6 where the models LG-45-LO and LG-45-HI are compared. The effect of the larger ram pressure is dramatic: the galactic size is extremely reduced, and the lower superbubble lobe can not break out of the gaseous halo, while the upper lobe is extremely distorted and bended downstream.

5 DISCUSSION AND CONCLUSIONS

Here we briefly summarise and discuss the behaviour of the ISM and of the SN ejecta in our models. For a better understanding of our results we also simulated the evolution of galactic winds occurring in the usual model galaxies but now assumed at rest relative to the IGM ($\rho_{\rm IGM} = 2 \times 10^{-28}$ g cm^{-3}, $T_{\rm IGM} = 10^6$ K; REST models), or not surrounded by any IGM (FIELD models). The aim of these models is to obtain a more direct insight of the role played by the ram pressure comparing interesting quantities such as the ISM and ejecta mass content (see Figures 5 and 7) in otherwise identical galaxies. The efficiency of metal ejection is known to be sensitive to the details of numerical simulations (cf. D'Ercole & Brighenti 1999 and MacLow & Ferrara 1999), and a consistent comparison must be done among similar models.

5.1 ISM evolution

The ISM of SM galaxies subject to the high ram pressure is quickly dragged away and therefore we did not simulate winds for SM-HI models. The low ram pressure strips only $30 - 50$ % of the original ISM of small galaxies (SM-LO models). However, the starburst powered wind completely removes all the gas in ≈ 100 Myr, a result obtained also by the galaxy at rest. Evidently the ram pressure has a negligible influence on the galactic wind evolution for these models. For more massive galaxies the occurrence of a starburst does not influence significantly the ongoing mass loss due to the ram pressure in the MD-LO models and can only anticipate the complete removal of gas (e.g. for model MD-00-HI).

For the more massive LG galaxies the situation is complicated by the radiative nature of the gaseous halo which develops around the galactic disk, especially in the edge-on model with the larger ram pressure (LG-00-HI). Cooling of the ablated gas makes $M_{\rm centr}$ to increase by a factor of few; $M_{\rm gal}$, instead, is not affected. As for the other models, the occurrence of a starburst in models LG does not influence the time evolution of $M_{\rm gal}$, which is determined by the ram pressure in both the HI and LO cases. We stress that in these models, as well as in any other model in which the galaxy is not rapidly deprived of gas by the wind, the ISM loses memory of the starburst after a few tens of Myr and recovers a distribution similar to the initial one. At this point the galaxy is in principle ready for another possible starburst episode.

In conclusion, our models show that the galactic wind either disrupts the whole ISM or has a negligible effect on the ISM content, which in turn is regulated mainly by the ram pressure. When $\rho_{\rm IGM} v_{\rm IGM}^2 \sim P_0$, where P_0 is the central ISM thermal pressure, the ram pressure stripping and the wind act together to increase the ISM removal rate. Many parameters regulate the ISM dynamics in this case (intensity and duration of the ram pressure, wind mechanical luminosity, potential well depth, initial amount of the ISM, value of the inclination angle θ) and numerical simulations are needed to understand the ISM behaviour of a specific model.

5.2 Ejecta evolution

For our low mass galaxies (models SM) the wind expels the whole ISM and no ejecta remains trapped into them. The more massive models with the lower ram pressure (MD-LO models) retain 5% of the total ejecta mass in the central region, and 10% in the whole galaxy. These are essentially the same values obtained by the analogous REST model, while for the analogous FIELD model the trapped quantities are lower by a factor of ~ 2. We thus conclude that for these models the ram pressure has little effect in the entrapment of the SN metals, while the presence of a relatively high pres-

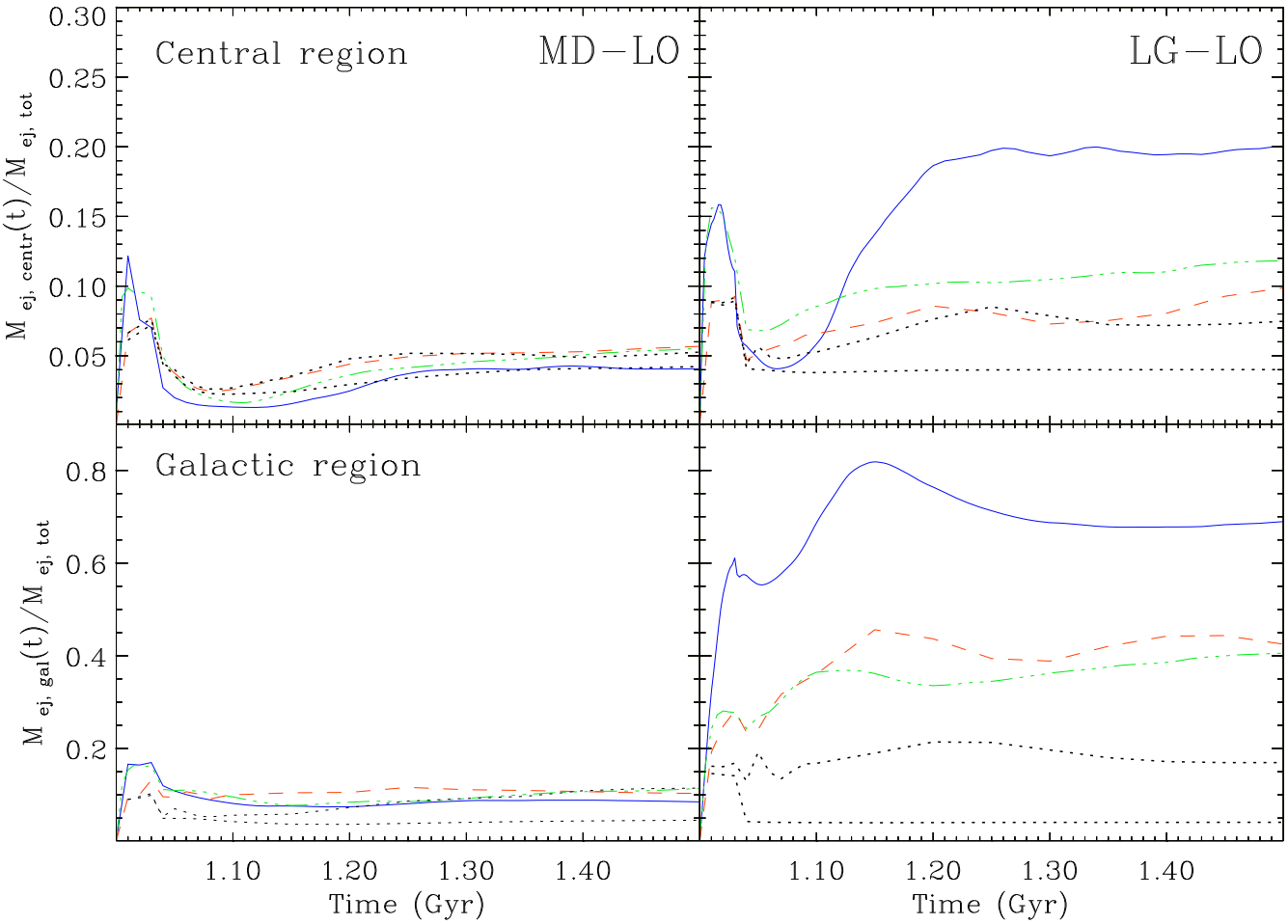

Figure 7. Evolution of the tracer in the central region (upper panels) and in the galactic region (lower panels). From left to right the couples of lower and upper panels refer to MD and LG models, respectively, in the case of lower ram pressure (LO). Solid blue lines: edge-on models; dashed-dotted green lines: 45° models; dashed red lines: face-on models. Higher and lower dotted lines in each panel represent the FIELD and REST models, respectively.

sure ambient gas helps this task. These results are in qualitative agreement with those in Murakami & Babul (1999). A quantitative comparison with the models by Murakami & Babul however is not possible. In fact, having these authors considered a spherical galaxy, the (metal rich) superbubble preserves a spherical shape when the ram pressure is negligible, and collapses as a whole. Thus, all the metals produced by the starburst are retained by the galaxy. On the other hand, in our flattened galaxies a large fraction of the ejecta is always lost through the superbubble breakout.

With the larger ram pressure, the ejecta and the ISM in the edge-on model MD-00-HI (the only model which keeps some ISM at the end of the ram pressure phase) are stripped after $t \sim 200$ Myr (Figure 8). For $t < 100$ Myr, however, the time evolution of the ejecta masses in both the central and galactic region is remarkably similar to that of model MD-00-LO. If the starburst occurs when the values of $M_{\rm centr}$ is high (model MDbis) more ejecta gets trapped, peaking at $t \simeq 30$ Myr with values of 20% and 55% in the central and galactic region, respectively. Then it decreases to 5% and 10% in the two regions.

The deeper potential well and the larger ISM amount of the LG-LO models are not the direct cause of the larger retention of metals with respect to the MD-LO galaxies, as can be verified comparing the FIELD and REST models for the LG and MD galaxies. Thus, the larger fraction of trapped metals occurring in the moving LG models is due to the presence of the extraplanar gaseous halo which develops in these models (in the edge-on case in particular), especially with the larger ram pressure. For the weaker ram pressure we find that the edge-on model keeps 20% of the ejecta in the central region at the end, though goes through a minima at t=70 Myr with 5%. The rise of $M_{\rm ej,centr}$ after this time is due to the collapsing halo gas polluted by the metals carried by the wind. The halo is also responsible of the rather high value ($\sim$ 70 %) of the mass of the ejecta trapped in the whole galactic region of the LG-00-LO model. For different values of θ, the halo is less developed, and less metals are trapped: around 10% in the central region, and $\sim$ 40 % in the galactic region, with little differences for various values of θ.

For LG-HI models the halo is even more influential. Now

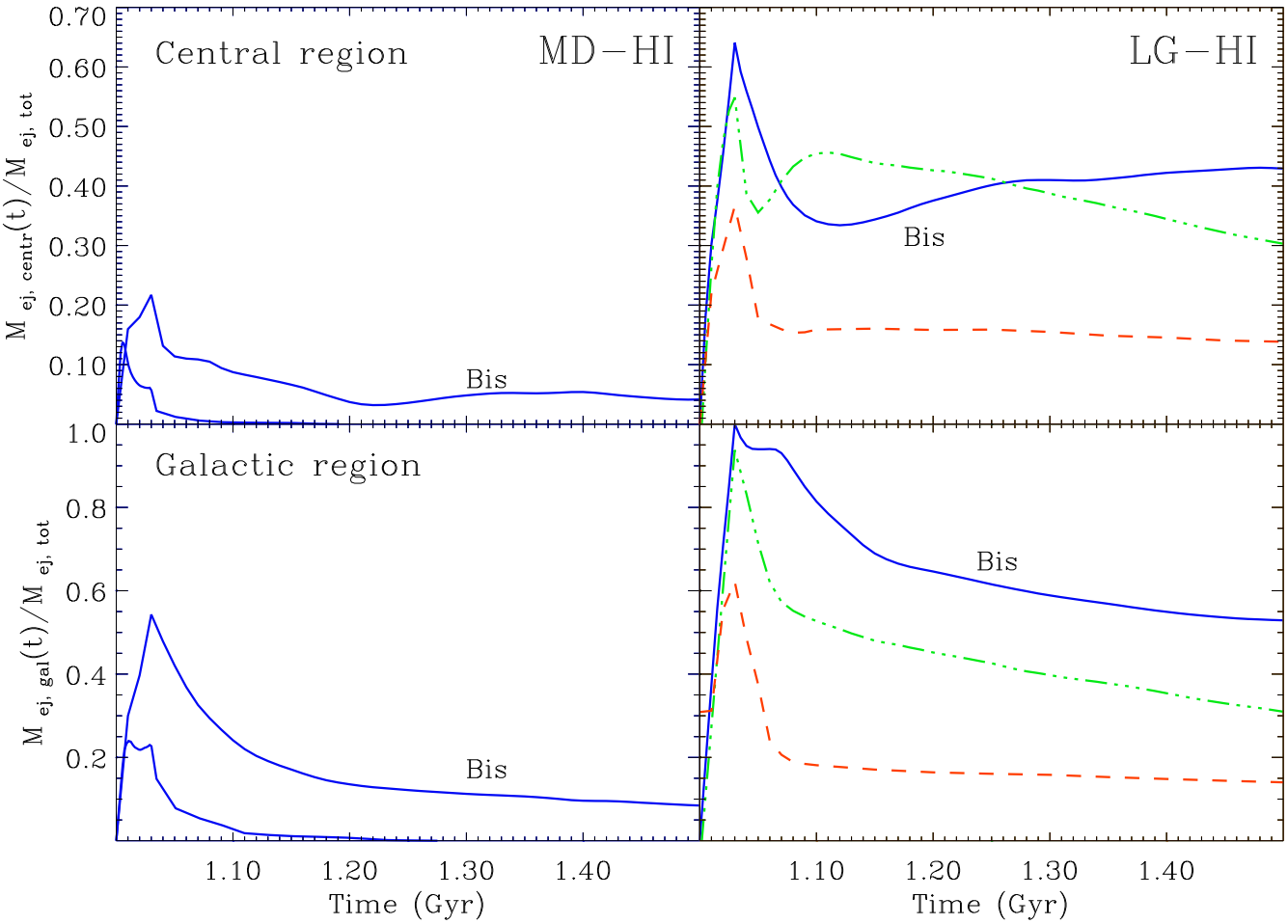

Figure 8. Evolution of the tracer in the central region (upper panels) and in the galactic region (lower panels). From left to right the couples of lower and upper panels refer to MD and LG models, respectively, in the case of higher ram pressure (HI). Solid lines: edge-on blue models; dashed-dotted green lines: 45° models; dashed red lines: face-on models.

the ejecta trapped in the central region is substantial: $\sim 43\%$ for $\theta = 0°$, $\sim 30\%$ for $\theta = 45°$, and $\sim 14\%$ for $\theta = 90°$. Very little ejecta is exterior to the central region, so the values of $M_{\rm ej,gal}$ are very similar to those of $M_{\rm ej,centr}$. Despite the presence of the more massive gaseous halo, $M_{\rm ej,gal}$ in the LG-HI models becomes somewhat lower than in the LG-LO models because of the stronger ram pressure which continuously erodes the polluted ISM.

We conclude that, contrary to the ISM dynamics, the amount of the SN ejecta trapped into the galaxy results to be more affected by the action of the ram pressure. Part of the ejecta expelled by the superwind is pushed back onto the galaxy by the incoming IGM or remains trapped in the surrounding halo, and the fraction of metals retained by a moving galaxy can be up to 3 times (depending on the value of θ) larger than that retained by a galaxy at rest. This trend is opposite to that found by Murakami & Babul (1999) in their suite of models, where they also investigated the effect of group-like ram pressure on galactic winds. This discrepancy is due to the assumed spherical ISM distribution of their models which allows the complete retention of the metals in the simulations without ram pressure.

Overall, the main conclusion by De Young & Heckman (1994), D'Ercole & Brighenti (1999) and Mac Low & Ferrara (1999) are not changed by the ram pressure stripping: for galaxies of size comparable to SM and MD only a very small fraction on the metals (of the order of ≈ 10 %) remains trapped in the ISM. Only the large models LG can trap much more ejecta, an effect of the relatively large amount of gas located at high z. This is conveyed there by the ram pressure and depends on the flare in the ISM distribution (we discuss this point in section 5.4). The (substantial) metal mass not incorporated in the ISM at $t = 500$ Myr is definitively lost by the galaxies and enriches the IGM, on spatial scales on the order of $30 - 50$ kpc. The general trend shown by our models is that the ram pressure increases $M_{\rm ej,centr}$ and $M_{\rm ej,gal}$.

To characterise the pollution degree we calculate the average ejecta fraction in the central region defined as $\mathcal{Z} = M^{\rm cold}_{\rm ej,centr}/\ M_{\rm centr}$, where we consider only the cold fraction ($T < 10^5$ K) of the ejecta which is effectively trapped in the ISM. In order to obtain the abundance of a specific X-element, one has to scale the $\mathcal{Z}$ value by a factor $Z_{\rm X,ej}$ representing the abundance of the X-element in the SN ejecta.

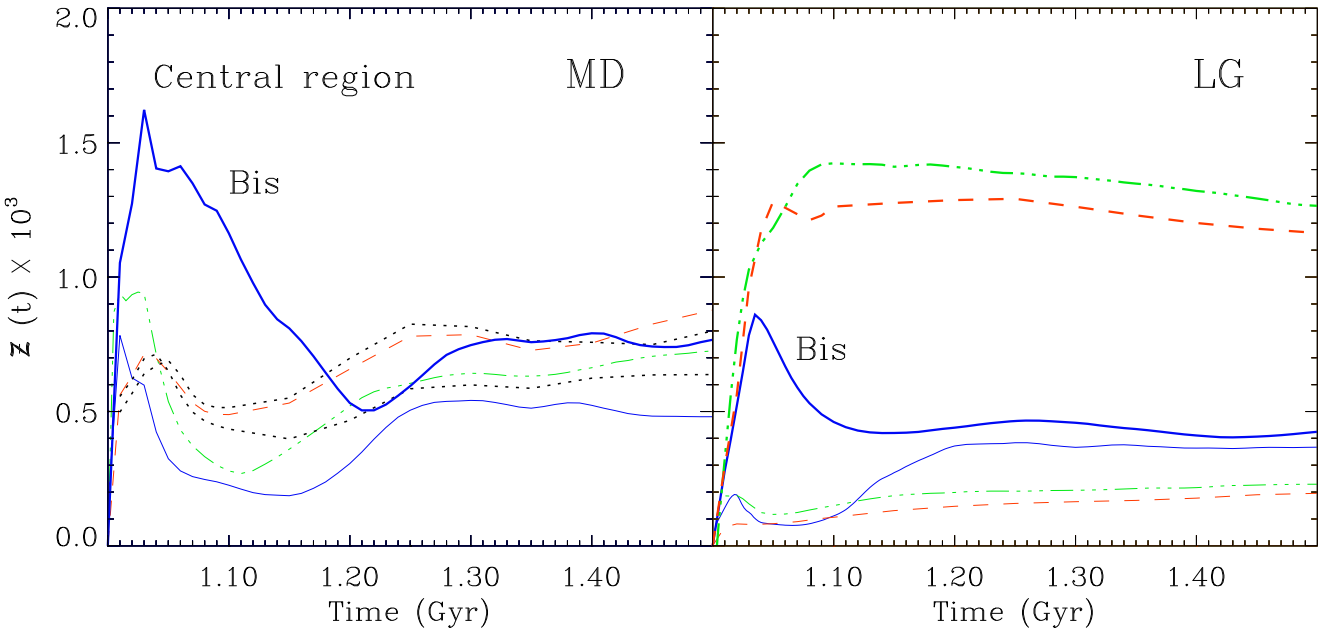

Figure 9. Evolution of $\mathcal{Z}$ (see text) in the central region. The left and right panel refer to MD and LG models, respectively. Solid blue lines: edge-on models; dashed-dotted green lines: 45° models; dashed red lines: face-on models. Higher and lower dotted lines in the right panel represent the FIELD and REST models, respectively. Light and heavy lines refer to LO and HI ram pressure models, respectively.

Focussing on iron and oxigen, we assume $Z_{\rm Fe,ej} = 4.4 \times 10^{-3}$ and $Z_{\rm O,ej} = 4.4 \times 10^{-2}$, and obtain $Z_{\rm Fe}/Z_{\rm Fe,\odot} = 3.4\mathcal{Z}$ and $Z_{\rm O}/Z_{\rm O,\odot} = 4.6\mathcal{Z}$, respectively (cf. D'Ercole & Brighenti 1999 for more details).

In Fig. 9 we show the evolution of $\mathcal{Z}$ in our models, and we note that in general larger ram pressures lead to an higher metal enrichment. Thus, the ability to retain metals appears to be sensitive to the parameters regulating the interaction ISM-IGM, and this may explain part of the observed scatter in the metallicity-luminosity relation (e.g. Lee, McCall & Richer 2003). We may also expect that dwarf irregulars in relatively high ram pressure environments have systematically larger metallicity than the field counterpart. Marginal evidence for such a trend has been claimed by Vilchez (1995) in his study of Virgo Irregulars. Elevated oxygen abundances for Virgo dwarfs has ben suggested also by Vilchez & Iglesias-Paramo (2003).

5.3 The gaseous halo

As discussed above the gas which accumulates at large z is a result of the ram pressure of the IGM with a flared ISM distribution. Its presence allows us to compare our results to those by Silich & Tenorio-Tagle (2001) and Legrand et al. (2001). These authors make a systematic study on the critical superwind luminosity needed for the superbubble to break out. They conclude that star-forming dwarf galaxies must have an extended gaseous halo in order retain their metals and enhance their abundances. A direct comparison between our edge-on models and the models by Silich & Tenorio-Tagle is prevented by the fact the galactic models are build following different criteria; the shape of the gaseous halo is also different. However, we consider two models by Silich & Tenorio-Tagle, their models M800.100 and M900.100, which have values of $M_{\rm g}$ and $M_{\rm h}$ similar to our MD and LG models, respectively. Moreover, the column density of the gaseous halo of these models during the edge-on stripping is also similar to the column density of the halo of the two quoted models by Silich & Tenorio-Tagle. Following these latter authors, the wind luminosity of our models is much larger than the critical luminosity needed by the superbubble to break out in the MD models. Thus the wind easily moves far from the galaxy bringing away most of the SNII ejecta. On the contrary, the wind luminosity would be only marginally sufficient to allow the breakout of the superbubble in the LG model. Actually, our simulations show that the superbubble breaks only marginally in this case, and the larger fraction of ejecta trapped in the galaxy (Fig. 7-8) indicates a more substantial role of the extraplanar gaseous halo.

5.4 Limitations of the models and future work

In evaluating the above results one must bear in mind the two caveats discussed above: *i*) the numerical diffusion, and *ii*) the flared ISM distribution. The numerical diffusion prevents the possibility to give an accurate *quantitative* estimate of the ejecta mixed with the ISM. However, we believe that the *relative* differences among the models are still meaningful, and thus ram pressure may indeed increase the metal enrichment of the ISM due to a starburst.

The metal enrichment in our models is also influenced by the ISM flare. This influence is particularly evident for large galaxies moving edge-on through the IGM (LG-00

models), where a gaseous halo form around the galaxy, affecting the superwind expansion. The flare in our models derives from the assumption of isothermal ISM, which requires a rotation curve independent of z in order to assure hydrostatic equilibrium (e.g. Tassoul 1978).

The real presence and the effective extension of flares in galaxies is still an open question, although evidence for flares in galaxies is claimed by several authors (e.g. Brinks & Burton 1984, Burton 1988, Olling 1996, Matthews & Wood 2003). Simulations analogous to those presented here but without flare in the initial ISM distribution would be interesting. We are currently devising non-isothermal models for the ISM to evaluate the real influence of the ISM distribution on the interaction with the IGM distribution.

ACKNOWLEDGEMENTS

We are grateful to the referee, Arif Babul, for a number of suggestions which improved the presentation of the paper. Many thanks to Renzo Sancisi for useful discussions on the ISM distribution. We acknowledge financial support from National Institute for Astrophysics (INAF). The simulations were run at the CINECA Supercomputing Centre with CPU time assigned thanks to INAF-CINECA grant.

REFERENCES

Babul A., Rees, M.J., 1992, MNRAS, 255, 346
Bateman N., Larson R., 1993, ApJ, 407, 634
Begelman M.C., Fabian A., 1990, MNRAS, 244, 26
Blumental G.R., Faber S. M., Primack J. R., Rees M. J., 1984, Nature, 311, 517
Bradamante F., Matteucci F., D'Ercole A., 1998, A&A, 337, 338
Brinks E., Burton W. B., 1984, A&A, 141, 195
Burton W.B., 1988, Galactic and Extragalactic radio Astronomy (2nd edition), Berlin and New York, Springer-Verlag, P. 295
de Avillez M., Mac Low M., 2002, ApJ, 581, 1047
De Young D.S., Heckman T. M., 1994, ApJ, 431, 598
Dekel A., Silk J., 1986, ApJ, 303, 39
Dekel A., Woo J., 2003, MNRAS, 344, 1131
della Ceca R., Griffiths R., Heckman T., 1997, ApJ, 485, 581
D'Ercole A., Brighenti F., 1999, MNRAS, 309, 941
Fields B., Olive K., 1998, ApJ, 506,177
Gallart C., Martinez-Delgado D., Gomez-Flechoso M.A., Mateo M., 2001, AJ, 121, 2572
Heckman T., 2003, RevMexAA (serie de Conferencias), 17, 47
Heckman T., Dahlem M., Lehnert M., Fabbiano G., Gilmore D., Waller W., 1995, ApJ, 448, 98
Kobulnicky H., Skillman E., 1996, ApJ, 471,211
Kobulnicky H., Skillman E., 1997, ApJ, 477, 679
Kobulnicky H., Skillman E., 1998, ApJ, 497, 601
Larsen T.I., Sommer-Larsen J., Pagel B., 2001, MNRAS, 323, 555
Lehnert M.D., Heckman T.M., Weaver K. A., 1999, ApJ, 523, 575
Legrand F., Tenorio-Tagle G., Silich S., Kunth D., Cervino M., 2001, ApJ, 560, 630
Leitherer C., Heckman T.M., 1995, ApJS, 96, 9
Koo B-C, McKee C. F., 1992, ApJ, 388, 93
Lee H., McCall M.L., Richer M.G., 2003, AJ, 125, 2975
Mac Low M.-M., Ferrara A., 1999, ApJ, 513, 142
Mac Low M.-M., McCray R., Norman M. L.,1989, ApJ, 337, 141
Marcolini A., Brighenti F., D'Ercole A., 2003, MNRAS, 345, 1329
Marconi G., Matteucci F., Tosi M., 1994, MNRAS, 270, 35
Martin C., 1998, ApJ, 506, 222
Martin C., 1999, ApJ, 513, 997
Martin C., Kobulnicky H., Heckman T., 2002, ApJ, 574, 663
Matteucci F., & Tosi M., 1985, MNRAS, 217, 391
Matthews L.D., Wood K., 2003, ApJ 593, 721
McKee C.F., Begelman M.C., 1990, ApJ, 358, 392
Murakami I., Babul A., 1999, MNRAS, 309, 161
Oey M.S., 2003, MNRAS, 339, 849
Olling R., 1996, AJ, 112, 457
Ott J., Walter F., Brinks E., Van Dyk S. D., Dirsch B., Klein U., 2001, AJ, 122, 3070
Pilyugin I. S., 1992, A&A, 260, 58
Quilis V., Moore B., Bower R., 2000, Sci, 288, 1617
Recchi S., Matteucci F., D'Ercole A., 2001, MNRAS, 322,800
Recchi S., Matteucci F., D'Ercole A., Tosi M., 2002, A&A, 384, 799
Roy J.-R., Kunth D., 1995, A&A, 294, 432
Silich S., Tenorio-Tagle G., 2001, MNRAS, 324, 191
Strickland D., Heckman T., Weaver K., Hoopes C., Dahlem M., 2002, ApJ, 568, 689
Strickland D., Stevens I., 2000, MNRAS, 327, 385
Suterland R., Dopita M., 1993, ApJS, 88, 253
Tassoul J-L. 1978, Theory of Rotating Stars, Princeton University Press
Tenorio-Tagle G., 1996, AJ, 111, 1641
Tully, R.B., 1987, ApJ, 321, 280
Vilchez J. M., 1995, AJ, 110, 1090
Vilchez J. M., Iglesias-Paramo J., 2003, ApJS, 145, 225
Vorobyov E. I., Klein U., Shchekinov Yu A., Ott J., astroph 0311164